Journal of Materials Chemistry C

ROYAL SOCIETY OF CHEMISTRY

PAPER

View Article Online
View Journal

Cite this: DOI: 10.1039/d5tc03406j

Spray-printing piezoresistive sensors based on poly(D,L-lactide-*co*-glycolide) copolymer composites for urinary catheter applications

E. Pimentel,[abc] R. Rodrigues,[ac] C. R. Tubio,[d] J. L. Vilaça,[ac] C. M. Costa,[be]* S. Lanceros-Méndez[bdf] and D. Miranda*[ac]

There is an increasing demand for new and improved methods for treating chronic diseases, such as Hinman syndrome or non-neurogenic bladder. Typically, a procedure called clean intermittent catheterization (CIC) is performed to remove urine by inserting a urinary catheter into the urethra, thereby relieving pressure on the bladder and preventing kidney damage. The placement of piezoresistive sensors in the urinary catheter can help optimize the insertion path during the procedure by monitoring the catheter's deformation along the urethra. Considering this, a sustainable approach was implemented for the development of biodegradable and biocompatible piezoresistive sensors based on the natural polymer poly(D,L-lactide-*co*-glycolide) (PDLG) with different contents of multiwalled carbon nanotubes (MWCNTs) up to 5 wt%. Their mechanical, electrical, thermal, morphological, and piezoresistive functional responses were assessed. The electrical percolation threshold occurred at a MWCNT content of 1 wt% and the maximum piezoresistive response was characterized by a gauge factor (GF) of ~1.5 for the same composite. The composite with 1 wt% MWCNT content was spray-printed onto the urinary catheter and the proof-of-concept implied the evaluation of the piezoresistive response of the sensor as a function of the catheter's deformation angle. The developed spray-printed piezoresistive sensors demonstrated suitable electrical, mechanical, and piezoresistive properties, offering an environmentally friendly and sustainable approach for the development of this type of biomedical device.

Received 12th September 2025,
Accepted 26th February 2026

DOI: 10.1039/d5tc03406j

rsc.li/materials-c

1. Introduction

There is a pressing societal challenge in the improvement of human well-being associated with increasing average life expectancy.[1] In particular, in western countries, the population aged 65 and over is growing very fast and the number will nearly double from 12% to 22% in the 2015–2050 period. Furthermore, 80% of older adults suffer from chronic diseases that require constant monitoring and treatment.[2] In each western economy, a large part of the gross domestic product (GDP) is attributed to health. Specifically, in the European union countries, the expenditure in this sector was the second largest item in 2021, representing 10.9% of the GDP.

On the other hand, the integration of digital methods in the health sector is being implemented at a high rate and represents a possible solution for the monitoring and treatment of different health conditions. The Internet of Things concept enables the use and interconnectivity of electronic devices that can capture specific and relevant health information.[3–5] This approach offers the opportunity for the development of smart devices that can bring direct information from and to the patient and reduce the need for the direct interaction between the patient and doctor, saving their time and reducing the overall cost of health procedures.[6–8]

Bladder diseases such as the Hinman syndrome or non-neurogenic bladder are voiding dysfunctions of the bladder of neuropsychological origin that is characterized by the absence of a neurological communication between the brain and the bladder, which causes an abnormal function of the latter,[9,10] and, if not properly treated, can lead to chronic renal insufficiency.[11] Typically, a procedure called clean intermittent catheterization (CIC) is performed to remove the urine *via* the

[a] 2Ai- School of Technology, IPCA, Barcelos, Portugal. E-mail: damiranda@ipca.pt
[b] Physics Centre of Minho and Porto Universities (CF-UM-UP) and Laboratory of Physics for Materials and Emergent Technologies, LapMET, University of Minho, 4710-057 Braga, Portugal. E-mail: cmscosta@fisica.uminho.pt
[c] LASI – Associate Laboratory of Intelligent Systems, Guimarães, Portugal
[d] BCMaterials, Basque Center for Materials, Applications and Nanostructures, UPV/EHU Science Park, 48940 Leioa, Spain
[e] IBS – Institute of Science and Innovation for Sustainability, University of Minho, 4710-057, Braga, Portugal
[f] IKERBASQUE, Basque Foundation for Science, 48009 Bilbao, Spain

introduction of a urinary catheter through the urethra, thereby alleviating pressure on the bladder and preventing kidney damage.[12,13] This method has a certain set of health complications, namely urethritis or inflammation of the urethral meatus due to the constant insertion of the catheter, urethral bleeding due to trauma, strictures or infections.[14,15] Epididymitis is a genital infection that widely occurs in men/children who have a urethral stricture.[16] These issues highlight the need for a solution and an upgrade of this procedure.

The incorporation of piezoresistive sensors represents a possible approach to functionalize catheters and improve the corresponding procedures through proper measurement and continuous evaluation, as they are already used in various biomedical applications and especially in urinary catheters.[17,18] Proper placement of piezoresistive sensors in urinary catheters enables the evaluation of the best path during the procedure to avoid possible health complications in the patient. Monitoring of this trajectory would represent an improvement in patients' quality of life.

Another major concern in today's society is environmental impact related to technological developments. In particular, there is an effort to replace, whenever possible, synthetic polymers originating from fossil fuels with natural polymers from renewable sources with low ecological footprint.[19] Biodegradable and biocompatible polymers are in high demand in the context of the transition to a circular economy.[20,21] Polylactic acid (PLA) is a thermoplastic aliphatic polyester widely used in a variety of applications, including in the biomedical field.[22,23] PLA is an ecofriendly, biocompatible and biodegradable material originating from natural sources such as sugar cane.[24] PLA offers unique advantages for the development of piezoresistive sensors, including its natural origin and environment-friendly nature. Furthermore, it is biocompatible and biodegradable, which is a relevant aspect when developing medical devices. This polymer enables the development of carbonaceous composites with tunable electrical conductivity. As an example, PLA with a 4% concentration of carbon nanotubes reaches the percolation threshold, which is achieved only at 7–10 wt% of graphene as a filler. The maximum electrical conductivity was 4–6 S m^{-1}. This is attributed to the higher aspect ratio (>1000) of CNTs with respect to graphene.[25]

Different stereochemical forms exist and impart specific mechanical and structural properties to the material depending on the L (laevorotatory) and D (dextrorotatory) isomer contents. By adding D-isomers to L-isomer based polymerization, poly-D,L-lactic acid (PDLA) is obtained.[26] Adjustment of the amount of the D and L isomers allows tuning of the biomechanical, thermal, rheological and biological properties of the material. A higher percentage of D-isomer leads to a higher disruption of the polymeric chain, which results in a higher degradation rate and a lower degree of crystallinity,[27] which allows tuning of the material for applications in which a faster resorption is desirable, such as drug delivery systems.[28] A 50 : 50 mixture of D- and L-isomers was selected in this work due to the extended resorption time, related to the D-isomer, and the enhanced mechanical properties, related to the L-isomer.[29] PLA can also be blended or copolymerized with different polymeric components, such as poly(glycolic acid) (PGA), for further tuning its properties. In this work, the most common PDLG composition with a 50 : 50 ratio of D,L-lactide/glycolide was selected due to its controlled degradation rates and customizable molecular weight, which allows tuning of biodegradability and biocompatibility. Furthermore, PDLG is an established polymer that has already been used in a range of biomedical applications, such as sustained drug delivery,[30] tissue engineering[31] and surgical implants.[32] The aim of this study was to develop piezoresistive printable sensors based on PDLG with different percentages of MWCNTs, which endow them with electrical and mechano-electrical properties, making them suitable for implementation in biomedical devices, such as urinary catheters.

2. Experimental details

2.1. Materials and methods

The polymer Purasorb PDLG with D/L-lactide and glycolide components in a 50 : 50 molar ratio and an inherent viscosity of 0.4 dl g^{-1} was supplied by Corbion. Multiwalled carbon nanotubes (MWCNTs) with reference NC7000 were purchased from Nanocyl. The MWCNTs had an average diameter of 9.5 nm, a length of 1.5 μm and a carbon purity of 90%. The solvent chloroform was obtained from Sigma-Aldrich.

2.2. Materials processing

The composites were prepared with different percentages (0, 1, 3, and 5 wt%) of MWCNTs. First, the corresponding MWCNT content was dispersed in chloroform in an ultrasound bath (ATU, model: ATM 40-3LCD) for 3 h at room temperature. Then, the polymer PDLG 50/50 was added in a specific solvent ratio of 1 : 5 (g mL^{-1}), and the solution was magnetically stirred at room temperature until the polymer was completely dissolved.

Then, the solutions were poured onto a glass substrate and spread using an extensor to obtain uniform films. After solvent evaporation at 25 °C, films with an average thickness of 50 μm were obtained.

The preparation procedure is presented in Fig. 1.

2.3. Characterization techniques

2.3.1. Physical–chemical characterization. Scanning electron microscopy (SEM) was carried out using a Hitachi S-4800 system to evaluate the morphology of the samples as well as the distribution of the MWCNTs within the polymer. Images of cross sections were acquired at a 5000× magnification.

Fourier transform infrared spectroscopy at room temperature was performed with a Jasco FT/IR-4100 system in the attenuated total reflectance mode (ATR). FTIR spectra were obtained between 600 and 4000 cm^{-1} at a scan resolution of 4 cm^{-1}.

X-ray diffraction (XRD) was used to examine the composites' structures. Experiments were performed using a Philips X'Pert

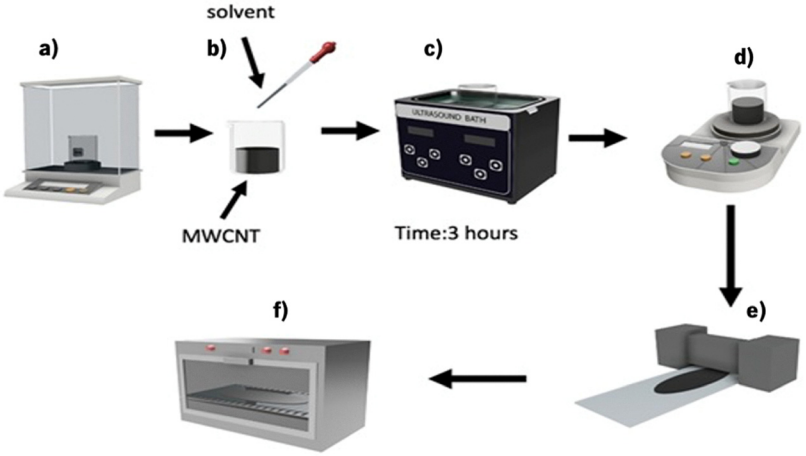

Fig. 1 Schematic representation of the processing of the PDLG piezoresistive composite films: (a) weighing of the polymer and fillers; (b) addition of chloroform and MWCNTs; (c) ultrasound bath for a period of 3 hours; (d) mixing of the solvent with the MWCNTs and the polymer; (e) doctor blade technique for the development of the films; and (f) evaporation of the solvent.

Pro diffractometer with Cu Kα radiation (λ = 1.5418 Å) and a step size of 0.001°.

Differential scanning calorimetry was used to evaluate the thermal characteristics of the samples using a DSC 3+ equipment. Experiments were carried out from 30 to 230 °C at a rate of 10 °C min^{-1} in a dry nitrogen atmosphere.

Mechanical testing in the tensile mode was performed using a Shimadzu AG-IS with a 500 N load cell. The samples were prepared in rectangular shapes with dimensions of 5 × 10 mm^2 and a thickness of approximately 50 μm, and measurements were carried out at a deformation rate of 5 mm min^{-1}. Three separate samples at each MWCNT concentration were used to determine the Young's modulus from stress–strain measurements up to 5% strain.

An automatic Keithley 6487 picoammeter/voltage source was used to measure the current–voltage (I–V) response by applying voltage (V) increments of 0.1 V from −1 to +1 V and measuring the current (I). The volume electrical resistance (R) was determined using gold electrodes (5 mm diameter) deposited (Polaron SC502 sputter coater) on both sides of the sample in a parallel configuration. The electrical conductivity (σ) was determined using eqn (1):

$$\sigma = \frac{d}{(R \times A)} \quad (1)$$

where d is the sample thickness and A is the area of the electrodes.

2.3.2. Piezoresistive functional characterization. Piezoresistive tests were performed in the 4-point bending mode as described in ref. 33. The composites were adhered to a 1.03 mm thick flexible polypropylene polymer substrate. Agar Scientific silver ink was used to print two electrodes on the composite with an area of 25 mm × 11 mm and an average thickness of 0.18 mm, and the distance between them was 29.02 mm. The electromechanical response of the samples was assessed between 1 and 5 mm of bending at various deformation rates (1 to 5 mm min^{-1}).

Eqn (2) was used to evaluate the composites' piezoresistive sensitivity (gauge factor, GF):

$$\mathrm{GF} = \frac{\Delta R/R_0}{\varepsilon} \quad (2)$$

where R_0 is the initial resistance, ΔR is the variation of resistance under mechanical deformation, and ε is the applied strain, which can be obtained using the theory of pure bending[34] (eqn (3)):

$$\varepsilon = \frac{3dz}{5a^2} \quad (3)$$

where a is the distance between electrodes (15 mm), z is the vertical displacement, up to 5 mm, and d is the thickness of the support and the sample (d = 1.048 mm).

2.4. Prototype development and characterization

Spray printing was used to demonstrate an easy, cost-effective and scalable way to print inks onto a 30 cm long Lofric Origo urinary catheter, typically used to completely empty a child's bladder. The ink containing 1 wt% MWCNTs was selected based on the electrical and piezoresistive characteristics. The biomedical device was placed on a wooden stand to ensure its stability and the piezoresistive inks were printed using an airbrush gun and an air compressor, as shown in Fig. 2a.

After printing, the catheter was placed in an oven (JSelecta, model no. 2000208) at a temperature of 70 °C (evaporation temperature of chloroform) for 10 minutes in order to evaporate all the solvent present in the substrate. Two conductive silver ink electrodes of dimensions 25 mm × 11 mm × 0.18 mm were deposited at a distance of 29.02 mm with the use of a brush and a copper wire was connected to them using a conductive electric ink (bare conductive with a sheet resistance of 55 Ω sq^{-1} at 50 μm film thickness).

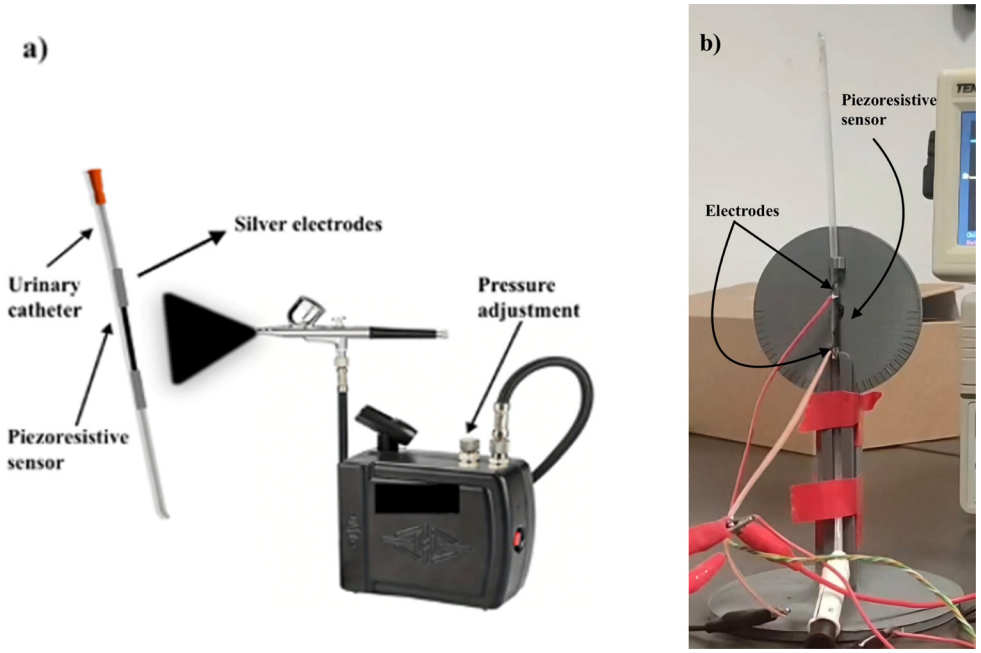

Fig. 2 (a) Spray printing of the piezoresistive sensors based on inks with 1 wt% MWCNT content on the Lofric Origo urinary catheter and (b) the urinary catheter with the developed piezoresistive sensors placed in the angle measurement device.

The piezoresistive response of the sensor printed on the urinary catheter was evaluated using an angle measure device (Fig. 3a), simulating the monitoring of the urinary catheter during the trajectory in clean intermittent catheterization.[35] Thus, the normal procedure of inserting a catheter into the urethra was simulated, allowing the study of the voltage variation (V) as a function of the catheter angle variation. For signal acquisition, a Wheatstone bridge (Fig. 3b) was developed. On one side, two 47 kΩ resistors are placed, whereas on the other side the piezoresistive sensor is placed, together with a potentiometer to help adjust the bridge output (Fig. 3). The bridge output is connected to a differential amplifier that subtracts the value of the two sides of the bridge and amplifies the signal. The signal is then delivered to the microcontroller (ATmega328) that receives and processes the raw data. Finally, an application was developed in Python to read the data through Serial Peripheral Interface (SPI) and save it in a computer (Fig. 3c).

Overall, considering the piezoresistive response of the sensor, the voltage variation was obtained as a function of the deformation angle.

3. Results and discussion

3.1. Morphology, vibrational spectra, and thermal and mechanical characteristics

The morphology of the composites and the dispersion of the MWCNTs in the PDLG polymer matrix were examined by SEM of their cross-sections, as shown in Fig. 4. The inclusion of carbon nanotubes in the samples 0MWCNT/PDLG, 1MWCNT/PDLG, and 3MWCNT/PDLG has no effect on the samples'

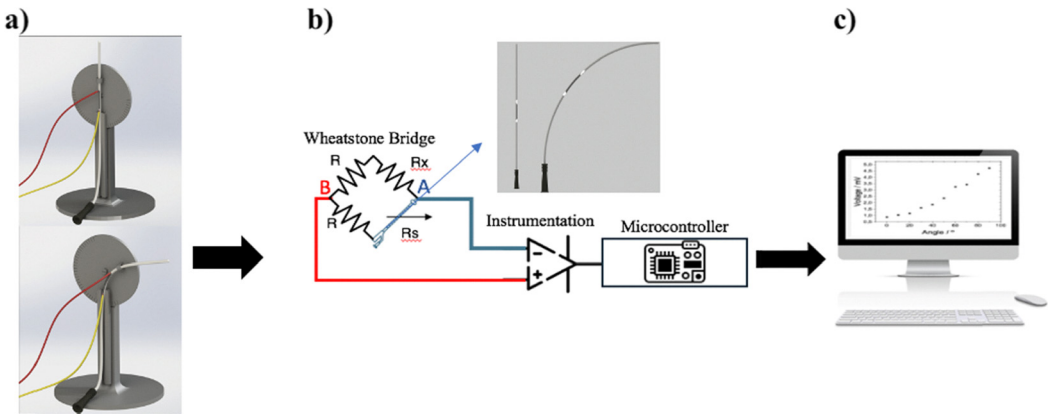

Fig. 3 (a) Schematic representation of the angle measure device, (b) the electronic acquisition circuit and (c) the corresponding computer analysis.

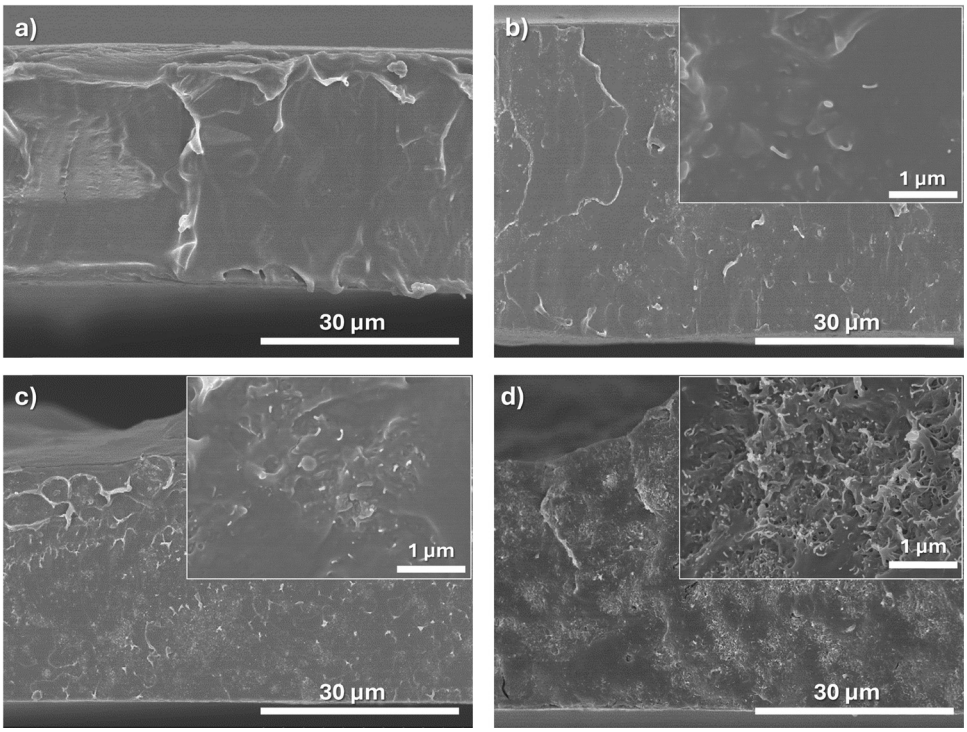

Fig. 4 Cross-sectional SEM images of (a) 0MWCNT/PDLG, (b) 1MWCNT/PDLG, (c) 3MWCNT/PDLG, and (d) 5MWCNT/PDLG. The insets show the same images at higher magnification.

morphology, which maintains a compact microstructure without voids, similar to that of the pristine polymers. However, the 5MWCNT/PDLG sample shows an increase in roughness and surface morphology, attributed to larger MWCNT agglomerates at this highest filler concentration.

Furthermore, the MWCNTs are evenly dispersed throughout the matrix with no large aggregates and good wettability between MWCNTs and the polymer, with no voids detected around the MWCNTs.

The interaction between the polymer and MWCNTs is typically driven by non-covalent weak forces, specifically van der Waals forces and mechanical interlocking, which creates interfacial adhesion, dispersion and reinforcement. In the specific case of PLA derived polymers, carbon nanotubes tend to effectively block the passage of water molecules into the polymer matrix due to their hydrophobic properties.[36]

The vibrational spectra of the composites obtained through FTIR-ATR experiments are displayed in Fig. 5a. The vibrational modes of the PDLG polymer are found to be unaffected by the MWCNT inclusion and content. Because of the stretching of the carbonyl groups in both D- and L-lactide monomers, the primary vibration peak is observed in the area between 1760 and 1750 cm^{-1} in all samples. Additionally, the asymmetric and symmetric C–C(=O)–O vibrations associated with the PDLG polymer are responsible for the detection of different stretching bands in the range between 1300 and 1150 cm^{-1}.[37] No new vibration bands or shift of bands are observed, indicating that no chemical interactions occur between the filler and polymer matrix.

The XRD patterns of neat PDLG and composites are shown in Fig. 5b. Low-intensity peaks in the θ range of 10–25° correspond to a dome-shaped region, indicating that all samples are primarily amorphous.[38] Moreover, MWCNTs have an impact on the peaks, intensifying them when added to the polymer matrix.

Fig. 5c displays the DSC curves of both neat PDLG and composites. No melting phase transition is observed in line with the amorphous nature of the films and with the literature, as the addition of MWCNTs to the polymer matrix does not increase the crystallinity of the films.[37]

The mechanical behavior of neat PDLG and composites with different MWCNT contents is shown in Fig. 5d. Fig. 5d depicts the typical mechanical behavior of a thermoplastic polymer and shows that the Young's modulus and maximum strain and stress are impacted by the inclusion of MWCNTs.

Using the secant method at 2% strain, the calculated values of Young's modulus in the elastic area range between 170 MPa for neat PDLG and 160 MPa for the 5 wt% composite.

According to the literature, it is expected that the Young's modulus increases at low filler concentrations (<1–2 wt%), as low filler concentrations act as mechanical reinforcement, whereas higher CNT concentrations lead to a decrease in the Young's modulus, as the fillers tend to act as defects under mechanical loading.[39] This is also corroborated by the general decrease of the maximum yield stress and deformation strain upon the inclusion of the MWCNTs. In the present case, the Young's modulus is similar for all samples, with variations falling within the experimental error.

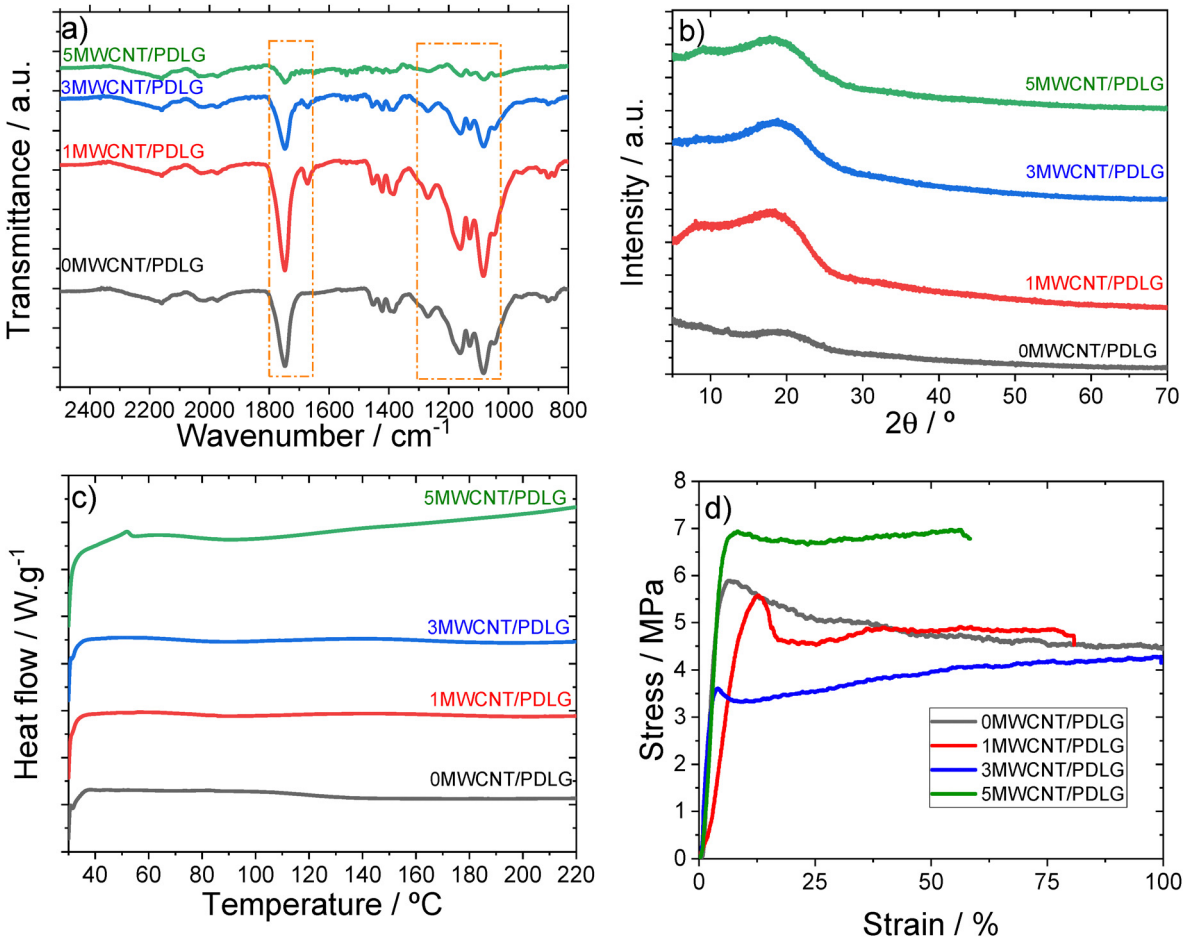

Fig. 5 (a) FTIR spectra, (b) X-ray diffraction patterns, (c) DSC curves and (d) stress–strain mechanical results of the composites based on PDLG polymers with different MWCNT contents.

In any case, the flexibility of the composites is maintained, and their mechanical properties are suitable for piezoresistive applications.

3.2. Electrical and piezoresistive characterization

The *I–V* curves of the PDLG polymer matrix and the composites are characterized by a linear (ohmic) behavior, as displayed in Fig. 6a. The addition of increasing MWCNT filler content to the polymer matrix increases the slope of the *I–V* curves, indicating the increase of electrical conductivity.[40] The electrical conductivity (σ) value was determined using eqn (1), and Fig. 6b displays the value of σ as a function of the MWCNT content. A maximum σ value of 8.6×10^{-4} S m^{-1} is obtained for the composite with 5 wt% MWCNT content, making the composites electrically conductive, in contrast to the dielectric behavior of the polymer matrix, with an electrical conductivity of 1.2×10^{-13} S m^{-1}. The electrical percolation threshold, which depends on the characteristics of the filler and matrix,[41] occurs below 2 wt% MWCNT content in the present case, indicating the suitable dispersion of the fillers.

Based on their mechanical and electrical data, the materials exhibit great potential for piezoresistive applications, as shown in Fig. 7a–c.

Piezoresistive sensors exhibit electrical resistance variations under mechanical stress or deformation, with the piezoelectric sensitivity of polymer composites being maximized around the percolation threshold or slightly above it.[42,43] For the composites with varying MWCNT contents, the piezoresistive response was evaluated under mechanical bending with maximum strain ranging from 1% to 5% and at different strain rates.

Fig. 7a displays the piezoresistive response of the polymer composites containing 1, 2, and 3 wt% MWCNT contents for 10 loading–unloading cycles at a maximum strain of 5% and a strain rate of 1 mm min^{-1}.

The MWCNT content that affects electrical and mechanical behavior and the interactions between the filler and the polymer determines this behavior, as shown in Fig. 7a. It is observed that increasing bending deformation leads to an increase in electrical resistance, whereas releasing the deformation leads to a decrease in resistance. Despite an overall variation of the maximum and minimum resistance over cycling, the obtained GF remains constant (within the experimental error) over cycling. Additionally, a second peak in the piezoresistive behavior is observed in the relaxation curves (sample unloading) (Fig. 7a) as a result of the rearrangement of the conductive network.[44] Once the polymer matrix

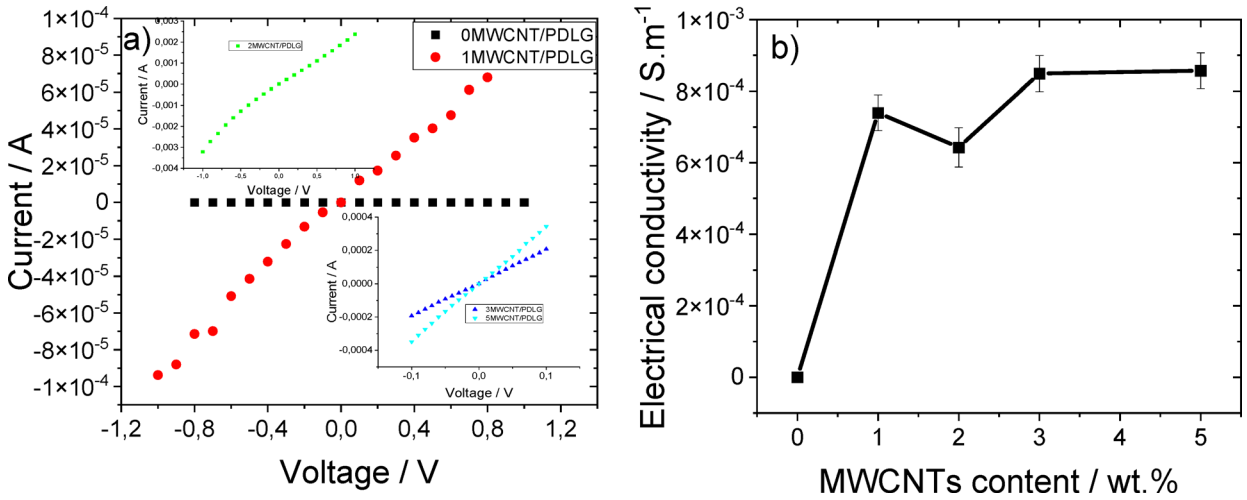

Fig. 6 (a) *I*–*V* curves and (b) electrical conductivity of the composites.

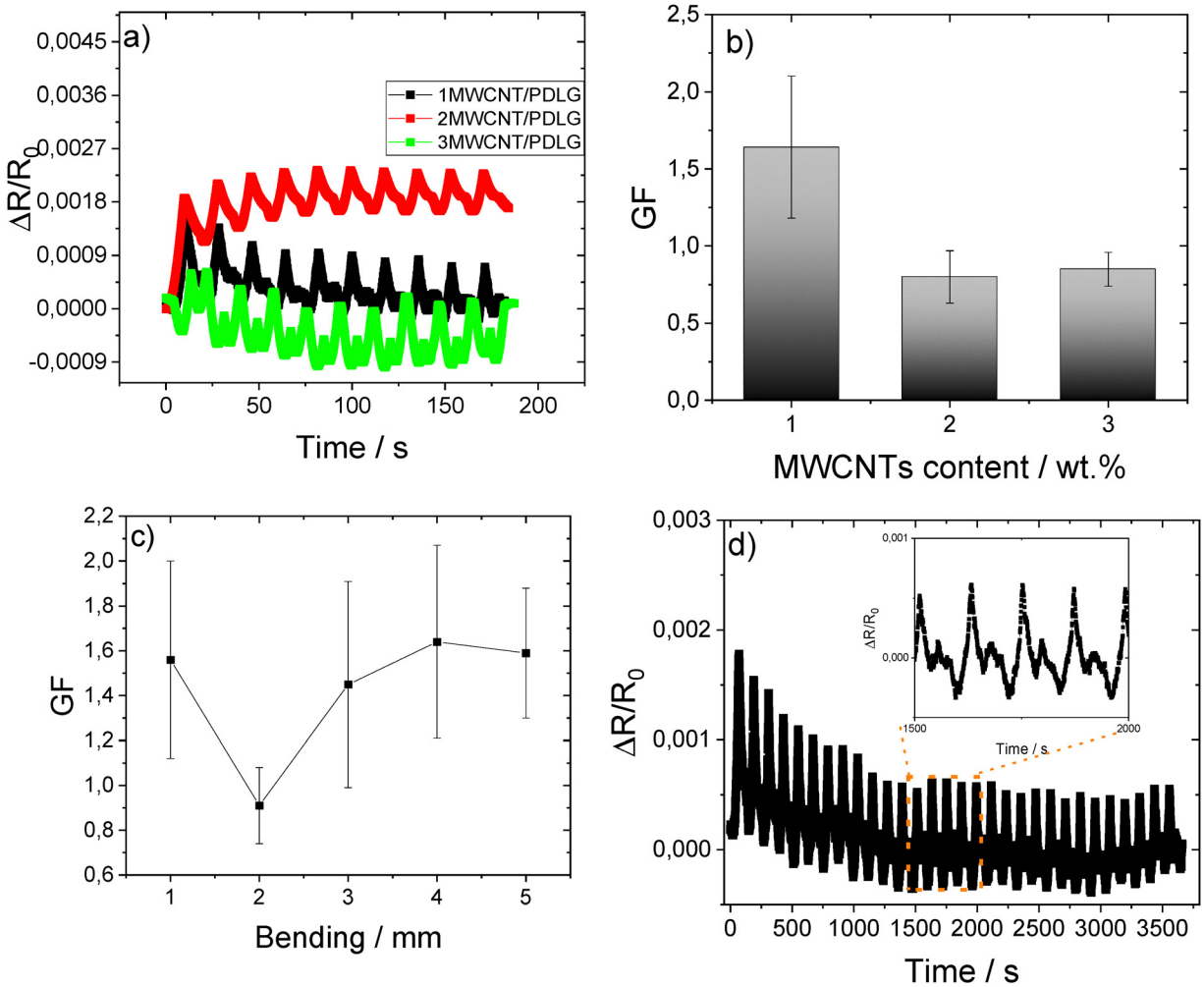

Fig. 7 (a) Piezoresistive bending behavior and (b) gauge factor for 10 bending loading–unloading cycles at v = 1 mm min^{-1} for the PDLG composites with 1, 2 and 3 wt% MWCNTs. (c) Gauge factor value of the PDLG composite with 1 wt% MWCNTs and (d) piezoresistive bending behavior of the 1 wt% MWCNT sample at 5 mm min^{-1} bending speed for 30 cycles.

exhibits viscoelasticity, which combines elastic (spring-like) and viscous (flow-like) qualities, this dynamic rearrangement may result in the creation, disruption, or modification of conductive pathways, which will affect the resistance of the

composite.[45] The presented results are similar for all applied maximum strains.

The gauge factor (GF) of the composites with 1, 2, and 3 wt% MWCNT contents is shown in Fig. 7b, which ranges from 0.9 to 1.6. The composite containing 1 wt% MWCNT content represents the best GF sample because of its electrical conductivity that allows greater resistance variation. Fig. 7c shows the piezoresistive sensitivity of the composite containing 1 wt% MWCNT content under bending between 1 and 5 mm, showing a value around 0.9–1.6. The GF values for strains ranging from 1 to 5 mm in these samples are around 1.6 for most of the samples, except for the sample with 2 wt% MWCNT content, attributed to filler aggregates.

Fig. 7d shows the cycling stability of the response over 30 cycles, showing that despite overall relaxation of the resistance due to non-reversible filler network reconfigurations and internal stress relaxation in the samples,[46] the GF remains nearly constant during cycling.

According to previous works, the sensitivity of polymer-based piezoresistive sensors typically exhibits GF values above 2.[47] However, for natural polymers, these values tend to be lower. CMC/CNT polymer composites show GF values around 1.79.[48] The alignment of the MWCNTs can be taken into consideration for the improvement of the piezoresistive sensitivity. In conductive pathways, when a strain is applied perpendicular to the alignment direction of a conductive pathway, the geometrical variations lead to a drop in conductivity, leading to higher gauge factors.[49]

3.3. Prototype characterization

The 1MWCNT/PDLG composite was selected for the fabrication of the prototype due to the larger GF values when compared to the other samples. The 1MWCNT/PDLG composite was spray-printed on the catheter (Fig. 3). Fig. 8a shows the printed sensor's piezoresistive response in the Lofric Origo catheter under 5 mm lateral bending deformation of the tip over 10 cycles. Fig. 8a shows excellent linearity between the mechanical and electrical responses under mechanical bending (GF = 0.97), which is suitable for the application, and the behavior is comparable to that observed in the film (Fig. 7). The large initial variation in resistance in the first cycle and the subsequent increase in maximum and minimum resistance are due to irreversible reconfigurations of the conductive filler network, as mentioned previously.

Fig. 8b shows the voltage variation as a function of the bending angle. A progressive 10° variation was applied step by step and the signal variation was acquired and stored in a data acquisition system. The maximum angle (90°) was selected according to the normal procedure of catheter insertion into the urethra. The results show that there is an increase in voltage with increasing bending angle with excellent linearity ($r > 0.95$).

Given the behavior observed in Fig. 8, the printed PDLG composites allow the measurement of a commercial catheter's flexion movements in real time.

A long-term analysis was carried out, demonstrating the piezoresistive bending behavior at 3 mm min^{-1} and a maximum bending of 3 mm over 100 cycles, proving that the cycling stability is maintained.[50]

Table 1 compares the composites developed in this work with other piezoresistive sensors based on sustainable materials reported in the literature.

The composites developed in this work exhibit performance similar or superior to that of other materials reported in the literature, as shown in Table 1.

Table 1 shows that the developed materials exhibit potential for applications in the biomedical industry, enabling improved and less invasive patient care.

Regarding biocompatibility and cytotoxicity, MWCNT nanocomposites typically exhibited non-toxic behavior after 24 hours of incubation (viability greater than 70%), as reported in the literature.[54]

Nevertheless, in order to improve biocompatibility, the sensor can be encapsulated with medical grade biocompatible materials.

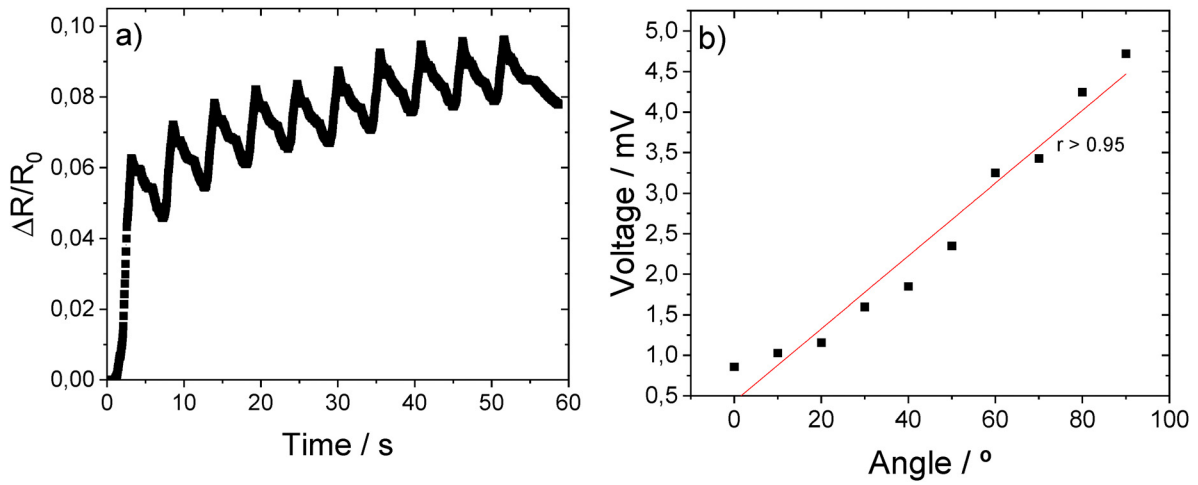

Fig. 8 (a) Piezoresistive response of the composite with 1 wt% MWCNT content applied to the catheter and (b) voltage variation of the catheter as a function of the bending angle.

Table 1 Piezoresistive composites based on sustainable materials

Composites	Electrical conductivity	Gauge factor	Flexibility	Sensitivity	Ref.
CMC/MWCNTs	0.1 S m^{-1}	GF ≈ 0.5	Pristine CMC presents a maximum strain of about 4% and a maximum stress of 50 MPa	—	48
Chitosan/CNTs	—	—	Maximum strain values of 10%, 20%, 30%, 40%, and 50% and maximum stress values of 42.3, 47.0, 61.5, 74.1 and 85.0 kPa were reached	494 kPa^{-1}	51
Ecoflex®/graphene nanoplatelet foams	Resistance = 17 KΩ	—	Maximum stress at each loading–unloading test was 90 kPa	0.28 kPa^{-1} for pressures lower than 10 kPa	52
Polypyrrole/cross-linked collagen sponge	2.4×10^{-3} S m^{-1}	GF = 0.16, 0.95, and 0.40 within the low-strain range (0–25%)	Maximum stress was around 300 kPa	—	53
PVA	The 5CNT/PVA composite presents the highest value of 0.11 S m^{-1}	GF ≈ 1.5	Maximum strain and stress near 100% and 20 MPa	—	48
MWCNT/PDLG	Maximum σ value of 8.6×10^{-4} S m^{-1} for 5% MWCNT content	GF ≈ 1.5	Young's modulus of 160 MPa for the 5 wt% composite	—	This work

4. Conclusions

Poly(D,L-lactide-*co*-glycolide) (PDLG) with different contents of multiwalled carbon nanotubes (MWCNTs; 0, 1, 2, 3, 4 and 5 wt%) was proven to be suitable for the development of piezoresistive sensors. The PDLG composites were developed by the solvent casting method and can be applied to biomedical devices by spray printing.

In terms of morphological characterization, no agglomerates and good dispersion of the MWCNTs were observed, providing suitable electrical properties for piezoresistive applications with a maximum electrical conductivity of 8.6×10^{-4} S m^{-1} and a percolation threshold below 2 wt% MWCNT content. The piezoresistive response of the composites shows a GF ranging from 0.9 to 1.6 under bending deformation.

1 wt% MWCNT/PDLG ink was spray-printed onto a urinary catheter to obtain a self-sensing device, allowing monitoring of bending motions through the corresponding electrical variations.

This work demonstrates that a natural polymer-based nanocomposite with suitable piezoresistive properties can be applied to urinary catheters and related biomedical applications.

Conflicts of interest

There are no conflicts to declare.

Data availability

The data that support the findings of this study are available from the corresponding author upon reasonable request.

Acknowledgements

The authors thank the Fundação para a Ciência e Tecnologia for financial support under the framework of the Strategic Funding UID/04650/2025 (https://doi.org/10.54499/UID/04650/2025), UIDB/05549/2020, UIDP/05549/2020, LASI-LA/P/0104/2020, and UIDB/00319/2020 and project SmartHealth, "NORTE-01-0145-FEDER-000045", supported by the Northern Portugal Regional Operational Programme (Norte2020), under the Portugal 2020 Partnership Agreement, through the European Regional Development Fund (ERDF). The authors also thank the FCT for financial support under individual research grant UI/BD/151058/2021 (E.P.). The authors acknowledge funding from the Basque Government Industry Department under the ELKARTEK program. This study is part of the Advanced Materials program and was supported by MCIN with funding from the European Union's NextGenerationEU (PRTR-C17.I1) and the Basque Government under the IKUR program. Technical and human support provided by Sgiker (UPV/EHU) and PCT-UBU are gratefully acknowledged.

References

1 L. Jong-Wook, *The Lancet*, 2003, **362**, 2083–2088.
2 P. Zhang, X. Zhang, J. Brown, D. Vistisen, R. Sicree, J. Shaw and G. Nichols, *Diabetes Res. Clin. Pract.*, 2010, **87**, 293–301.
3 M. Dadkhah, M. Mehraeen, F. Rahimnia and K. Kimiafar, *J. Med. Signals Sens.*, 2021, **11**, 138–157.
4 K. T. Kadhim, A. M. Alsahlany, S. M. Wadi and H. T. Kadhum, *Wirel. Pers. Commun.*, 2020, **114**, 2235–2262.
5 K. N. Swaroop, K. Chandu, R. Gorrepotu and S. Deb, *Internet of Things*, 2019, **5**, 116–129.
6 J. T. Kelly, K. L. Campbell, E. Gong and P. Scuffham, *J. Med. Int. Res.*, 2020, **22**, e20135.
7 G. Chen, X. Xiao, X. Zhao, T. Tat, M. Bick and J. Chen, *Chem. Rev.*, 2021, **122**, 3259–3291.
8 D. Furtado, A. F. Gygax, C. A. Chan and A. I. Bush, *Digit. Commun. Netw.*, 2023, **9**, 223–235.
9 T. D. Allen, *J. Urol.*, 1977, **117**, 232–238.
10 R. J. Nijman, *Curr. Opin. Urol.*, 2001, **11**, 577–583.
11 D. E. Varlam and J. Dippell, *Pediatr. Nephrol.*, 1995, **9**, 1–5.
12 J. Lapides, A. C. Diokno, S. M. Silber and B. S. Lowe, *J. Urol.*, 2002, **167**, 1584–1586.

13 V. P. Alencar, C. M. Gomes, E. P. Miranda, M. A. dos Santos Lelis, P. Fera, J. de Bessa Jr, M. Srougi and H. Bruschini, *Neurourol. Urodyn.*, 2018, **37**, 2833–2840.
14 J. Wyndaele, *Spinal Cord*, 2002, **40**, 536–541.
15 K. N. Moore, M. Fader and K. Getliffe, *Cochrane Database Syst. Rev.*, 2007, **4**, CD006008.
16 M. I. Baker, S. P. Walsh, Z. Schwartz and B. D. Boyan, *J. Biomed. Mater. Res., Part B*, 2012, **100**, 1451–1457.
17 K. Meena and A. R. Sankar, *IEEE Sens. J.*, 2021, **21**, 10241–10290.
18 M. Ahmadi, R. Rajamani, G. Timm and A. S. Sezen, *J. Microelectromech. Syst.*, 2015, **24**, 1840–1847.
19 N. Gowthaman, H. Lim, T. Sreeraj, A. Amalraj and S. Gopi, *Biopolymers and their Industrial Applications*, Elsevier, 2021, pp. 351–372.
20 B. Mrowiec, *Environ. Protect. Nat. Res.*, 2018, **29**, 16–19.
21 C. Matthews, F. Moran and A. K. Jaiswal, *J. Cleaner Prod.*, 2021, **283**, 125263.
22 F. Ebrahimi and H. Ramezani Dana, *Int. J. Polym. Mater. Polym. Biomater.*, 2022, **71**, 1117–1130.
23 M. Singhvi, S. Zinjarde and D. Gokhale, *J. Appl. Microbiol.*, 2019, **127**, 1612–1626.
24 G. Rajeshkumar, S. A. Seshadri, G. Devnani, M. Sanjay, S. Siengchin, J. P. Maran, N. A. Al-Dhabi, P. Karuppiah, V. A. Mariadhas and N. Sivarajasekar, *J. Cleaner Prod.*, 2021, **310**, 127483.
25 S. Guo, E. Ivanov, V. Georgiev, P. Stanley, I. Radecka, A. M. Eissa, R. Tolve and F. Tchuenbou-Magaia, *Polymers*, 2026, **18**, 99.
26 J. O. C. de França, D. da Silva Valadares, M. F. Paiva, S. C. L. Dias and J. A. Dias, *Polymers*, 2022, **14**, 2317.
27 M. Murariu, Y. Paint, O. Murariu, F. Laoutid and P. Dubois, *Polymers*, 2022, **14**, 2360.
28 Y. Su, B. Zhang, R. Sun, W. Liu, Q. Zhu, X. Zhang, R. Wang and C. Chen, *Drug Delivery*, 2021, **28**, 1397–1418.
29 M. Annunziata, L. Nastri, G. Cecoro and L. Guida, *Molecules*, 2017, **22**, 2214.
30 D. Essa, P. P. Kondiah, Y. E. Choonara and V. Pillay, *Front. Bioeng. Biotechnol.*, 2020, **8**, 48.
31 N. A. Akar, G. G. Peközer and G. Köse, *Turk. J. Biol.*, 2019, **43**, 235–245.
32 F. A. Barber and S. A. Hrnack, *J. Knee Surg.*, 2013, **26**, 423–428.
33 E. Pimentel, N. Pereira, P. Costa, C. R. Tubio, J. L. Vilaça, C. M. Costa, S. Lanceros-Méndez and D. Miranda, *J. Alloys Compd.*, 2025, **1034**, 181447.
34 A. Paleo, F. Van Hattum, J. Pereira, J. G. Rocha, J. Silva, V. Sencadas and S. Lanceros-Méndez, *Smart Mater. Struct.*, 2010, **19**, 065013.
35 S. H. Saadat, S. Shepherd, B. Van Asseldonk and D. S. Elterman, *Can. Urol. Assoc. J.*, 2018, **13**(2), 64–69.
36 M. M. Younus, H. M. Naguib, M. Fekry and M. A. Elsawy, *Sci. Rep.*, 2023, **13**, 16588.
37 C. D. A. C. Erbetta, R. J. Alves, J. Magalh, R. F. de Souza Freitas and R. G. de Sousa, 2012.
38 N. Mahajan, D. M. Sakarkar and A. Manmode, *Int. J. Pharm. Pharm. Sci.*, 2011, **3**, 208–214.
39 W.-S. Bae, O. J. Kwon, B. C. Kim and D. W. Chae, *Korea Aust. Rheol. J*, 2012, **24**, 221–227.
40 Q. Yang, L. Ma, S. Xiao, D. Zhang, A. Djoulde, M. Ye, Y. Lin, S. Geng, X. Li, T. Chen and L. Sun, *Nanomaterials*, 2021, **11**, 1290.
41 A. Oseli, T. Tomković, S. G. Hatzikiriakos, A. Vesel, M. Arzenšek, T. Rojac, M. Mihelčič and L. Slemenik Perše, *Compos. Sci. Technol.*, 2023, **237**, 110010.
42 M. Haghgoo, M. K. Hassanzadeh-Aghdam and R. Ansari, *Composites, Part A*, 2020, **130**, 105735.
43 S. Naderizadeh, G. Santagiuliana, W. Tu, D. Marsh, E. Bilotti and J. J. C. Busfield, *IEEE Sens. J.*, 2023, **23**, 18013–18021.
44 C.-Y. Tang, L. Liu, K. Ke, B. Yin, M.-B. Yang and W. Yang, *Nano Mater. Sci.*, 2023, **5**, 312–318.
45 C. Yan, D.-F. Hou, K. Zhang and M.-B. Yang, *Polymer*, 2023, **270**, 125764.
46 P. Costa, S. Gonçalves, H. Mora, S. A. C. Carabineiro, J. C. Viana and S. Lanceros-Mendez, *ACS Appl. Mater. Interfaces*, 2019, **11**, 46286–46295.
47 E. Pimentel, P. Costa, J. Vilaça, C. M. Costa, S. Lanceros-Méndez and D. Miranda, *React. Funct. Polym.*, 2025, **217**, 106502.
48 E. Pimentel, P. Costa, C. R. Tubio, J. L. Vilaça, C. M. Costa, S. Lanceros-Méndez and D. Miranda, *Compos. Sci. Technol.*, 2023, **239**, 110071.
49 H. Kim, S.-K. Hong, J.-K. Ryu and S.-H. Park, *Materials*, 2020, **13**, 2598.
50 E. Pimentel, S. G. Pereira, J. L. Vilaça, C. M. Costa, S. Lanceros-Méndez and D. Miranda, *Sens. Actuators, A*, 2026, **399**, 117483.
51 J. Wu, H. Li, X. Lai, Z. Chen and X. Zeng, *Chem. Eng. J.*, 2020, **386**, 123998.
52 M. Fortunato, I. Bellagamba, A. Tamburrano and M. S. Sarto, *Sensors*, 2020, **20**, 4406.
53 L. Liu, Y. Zhang, L. Tan, Y. Deng, X. Zheng, K. Tang and Y. Pei, *Chem. Eng. J.*, 2024, **499**, 155975.
54 T. L. D. A. Montanheiro, V. M. Schatkoski, D. E. M. Camarena, T. C. de Oliveira, D. M. da Silva, M. R. D. C. Vegian, L. H. Catalani, C. Y. Koga-Ito and G. P. Thim, *C*, 2024, **10**, 33.

